Front. Struct. Civ. Eng. 2022, 16(10): 1233–1248
https://doi.org/10.1007/s11709-022-0878-1

RESEARCH ARTICLE

Predicting the capacity of perfobond rib shear connector using an ANN model and GSA method

Guorui SUN[a,b], Jun SHI[a,c*], Yuang DENG[a]

[a] *School of Civil Engineering, Central South University, Changsha 410075, China*
[b] *Key Laboratory of Structures Dynamic Behavior and Control of the Ministry of Education, Harbin Institute of Technology, Harbin 150090, China*
[c] *National Engineering Laboratory for High-Speed Railway Construction, Changsha 410075, China*
[*] *Corresponding author. E-mail: csushijun@csu.edu.cn*

ABSTRACT Due to recent advances in the field of artificial neural networks (ANN) and the global sensitivity analysis (GSA) method, the application of these techniques in structural analysis has become feasible. A connector is an important part of a composite beam, and its shear strength can have a significant impact on structural design. In this paper, the shear performance of perfobond rib shear connectors (PRSCs) is predicted based on the back propagation (BP) ANN model, the Genetic Algorithm (GA) method and GSA method. A database was created using push-out test test and related references, where the input variables were based on different empirical formulas and the output variables were the corresponding shear strengths. The results predicted by the ANN models and empirical equations were compared, and the factors affecting shear strength were examined by the GSA method. The results show that the use of ANN model optimization by GA method has fewer errors compared to the empirical equations. Furthermore, penetrating reinforcement has the greatest sensitivity to shear performance, while the bonding force between steel plate and concrete has the least sensitivity to shear strength.

KEYWORDS perfobond rib shear connector, shear strength, ANN model, global sensitivity analysis

1 Introduction

The use of steel-concrete composite structures has increased in bridge structures due to their ability to take full advantage of the tensile strength of steel and the compressive strength of concrete [1–3]. Shear connectors are the key components for connecting different components and making them work together [4,5]. Commonly used shear connectors include section steel connectors, stud connectors and perfobond rib shear connectors (PRSCs). Compared with traditional connectors, PRSCs have the characteristics of easy processing, excellent mechanical properties and good fatigue performance.

PRSCs consist of steel sections, perforated steel plates, penetration reinforcement and concrete, and each of the components could affect its shear strength [6–10]. The research on PRSCs can be traced back to the 1980s, when the fabricating process of PRSCs was proposed [11]. It investigated the effect of perforated plates with different hole diameters on the bearing capacity. With the further research and development [12–15], it is found that the shear strength increases with the increase of the number of holes, concrete strength and reinforcement ratio. Zheng et al. [16,17] investigated the effect of hole shape on bearing capacity based on 72 push-out experimental specimens. PRSCs are key components of the composite beam and their shear capacity affects the structural design of the composite beam. However, most of them are based on the empirical equations obtained by linear regression of experimental data, and the accuracy of the calculation is greatly affected by the specific nature of the experiment [6–12]. Although the finite element method is widely used in forecasting, it still has shortcomings such as long implementation period, large output variance and large data demand.

Article history: Received Apr 5, 2022; Accepted Jun 7, 2022

Mathematical tools like artificial neural networks (ANN) help to solve complex questions without reproducing the phenomenon under study [18–25]. Due to recent developments in artificial intelligence and computer technology, the application of these techniques in structural analysis has become possible [26–30]. Hamdia et al. [31] employed genetic algorithm (GA)-based integer-valued optimization for two machine learning (ML) models and used this method to predict the fracture energy of polymer/nanoparticle composites (PNCs). Using an adaptive network-based fuzzy inference system (ANFIS) as a modeling technique, researchers predicted the shear strength of various connector types and analyzed the degree of influence of different variables on the bearing capacity [32,33]. With the continuous development of ANN, researchers have also started to use ANN models to calculate the bearing capacity of PRSCs [34]. Allahyari et al. [35] proposed a novel ANN-based numerical method to calculate the shear strength of connectors. The tests show that the ANN model has less computational error compared to the existing empirical equations. The shear strength prediction ability of different artificial intelligence methods for PRSCs was investigated by Khalaf et al. [36]. It was found that employing the GA method improved the accuracy of the ANN model through optimizing the removal of redundant variables that reduce the model's efficiency. Global sensitivity analysis (GSA) can analyze the impact of multiple parameters on the overall results of the model, and analyze the impact of individual parameters and their interactions on the results [37–39]. The GSA method could analyze the effect of different variables on the shear strength of concrete structures [40].

In summary, a great number of studies have been conducted to investigate the bearing capacity of PRSCs based on experimental and numerical simulation analysis. However, several issues still need to be solved, which are summarized as follows.

1) Compared with empirical equations, artificial intelligence models have higher prediction accuracy. However, fewer researchers have applied different ANN models to calculate the shear bearing capacity of PRSCs. It is necessary to study the prediction accuracy of different neural network models on shear bearing capacity resistance and select the appropriate prediction method.

2) The calculation results are mainly affected by the adopted method and the selected parameters, while the existing ANN models cannot quantitatively determine the influence of each selected parameter on the shear property. The GSA method can quantitatively analyze the role of each factor, but requires a large amount of data. Therefore, it is necessary to couple neural networks with the GSA method to choose the essential input parameters to improve the prediction accuracy.

The shear strength of PRSCs was investigated in this paper based on experiments, ANN models and GSA method. First, the roles of the number of holes and of the reinforcement on the shear property of PRSCs were investigated by nine push-out test specimens. The experimentally obtained shear strength was used as part of the ANN model test set to verify the prediction effect. Then, the influencing factors of shear strength were determined by considering previous references and empirical equations, and the ANN models with different input parameters were established. The computational accuracy of the ANN model was investigated by comparing the prediction results of different ANN models with empirical equations. Finally, a GSA method based on the ANN model was introduced, and each factor's sensitivity to shear strength was determined.

2 Experimental investigation

2.1 Specimens design

Nine specimens were fabricated according to Eurocode 4 [41] and DB 41/T 696-2011 standard [42], as shown in Fig. 1 and Table 1. Nine specimens, numbered N12-1 –N16-3, were prepared, where "N", "12" and "1" denoted normal strength concrete, diameter of penetrating rebars and number of rib holes per connector, respectively. The H-section steel was 300 mm × 300 mm × 10 mm × 15 mm, and the concrete slab was 60 mm × 600 mm × 150 mm. The type of steel plates were all Q345. The yield strength, ultimate strength and modulus of elasticity of the steel plates were 345 MPa, 570 MPa and 200 GPa, respectively. The diameter of the hole in steel plate was 40 mm. Penetrating rebars of length 450 mm were placed in each hole. The steel bars were all HRB400 type, with a yield strength of 400 MPa, ultimate strength of 570 MPa and elastic modulus of 200 GPa.

2.2 Loading setup and measurements system

All specimens were tested on a hydraulic testing machine with a capacity of 5000 kN. Left and right symmetrical displacement gauges were set at the bottom of the concrete slab and H-beam to detect the relative slip between the slab and the beam. The loading device is shown in Fig. 2. During the test, the loading was performed by displacement control (1 mm/min) until the specimen failed.

3 Analysis of test results

3.1 Failure modes

Due to the high strength of the steel plate used in the test,

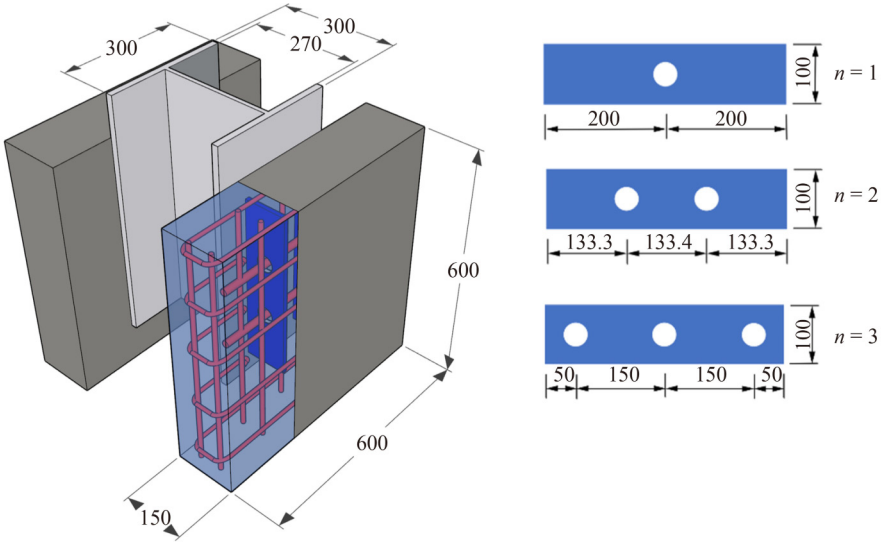

Fig. 1 The shape and size of the specimens (mm).

Table 1 Parameters of the specimen

specimens	f_c (MPa)	d_r (mm)	n
N12-3	53.7	12	3
N16-3	53.7	16	3
N20-3	53.7	20	3
N12-2	53.7	12	2
N16-2	53.7	16	2
N20-2	53.7	20	2
N12-1	53.7	12	1
N16-1	53.7	16	1
N20-1	53.7	20	1

Note: f_c is the compressive strength of concrete; d_r is the diameter of penetrating rebars; n is the number of rib holes per connector.

the steel plate was not damaged in the experiment. Damage models of specimens in this paper are mainly divided into two types, as shown in Fig. 3. When the diameter of the perforated reinforcement and the number of holes were small, such as was the case for specimens N12-1 and N16-1, the concrete in the hole was damaged first, and then the reinforcement fractured. When the diameter of the reinforcement in the hole or the number of holes was large, longitudinal splitting damage occurred in the concrete. During the loading condition, the cracks in the core concrete spread outward to the surface of the concrete slab, forming longitudinal splitting cracks along the location of the perforated steel plate, which rapidly developed and penetrated the concrete slab.

The crack distribution of the specimens is shown in Fig. 3(a). When the number of holes was small and the diameter of the penetrating reinforcement was small, the damage was mainly caused by the concrete tenons and reinforcement, so there was no significant damage to the external concrete slab, as shown for specimen N12-1.

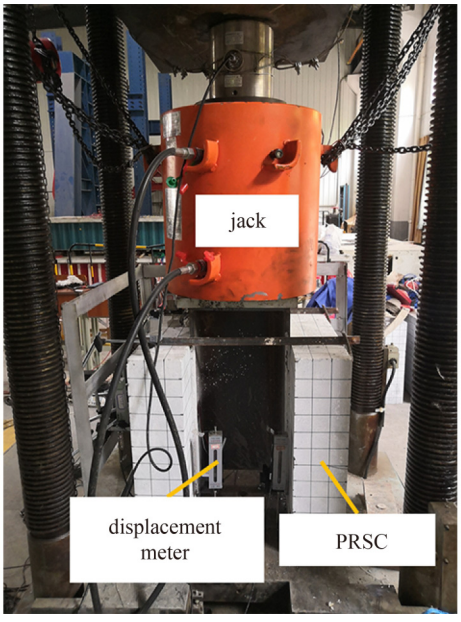

Fig. 2 Loading device.

When the bearing capacity in the hole of the perforated steel plate was large, the damage mainly occurred to the external concrete slab, as shown in the case of specimen N12-3. The main damage pattern of the reinforcement is shown in Fig. 3(b). With increase of the number of holes and the diameter of the reinforcement the damage of the reinforcement became less obvious.

3.2 Load-slip behavior

Taking the average value of displacement meter measurement on both sides as the horizontal coordinate and the load value of the testing machine as the vertical coordinate, the load-slip curve of the specimens is shown

in Fig. 4. As in other studies [2,3], the failure process of PRSC could be divided into four stages: elastic stage, plastic stage, yield strengthening stage, and failure stage. In the initial stage of loading, there was almost no relative sliding between the H-beam and the concrete slab. The stress in the specimen was quite small and the load increased linearly and rapidly in the elastic phase. After that, the displacement in the specimen gradually increased with the increase of the load. Cracks in the concrete gradually developed and the slope of the load-displacement curve decreased, at which point it was in the plastic phase. With further increase of the load, the growth rate of the load-displacement curve further decreased and entered the yield strengthening stage. Under the action of the load, a certain degree of deformation of the reinforcement and perforated steel plate occurred, and the stiffness of the joint was reduced accordingly. When the load reached the limit value, the connector failed and entered the failure stage. Similarly, the diameter of the reinforcement and the number of

Fig. 3 Failure mode: (a) damage of concrete slabs; (b) damage of reinforcement.

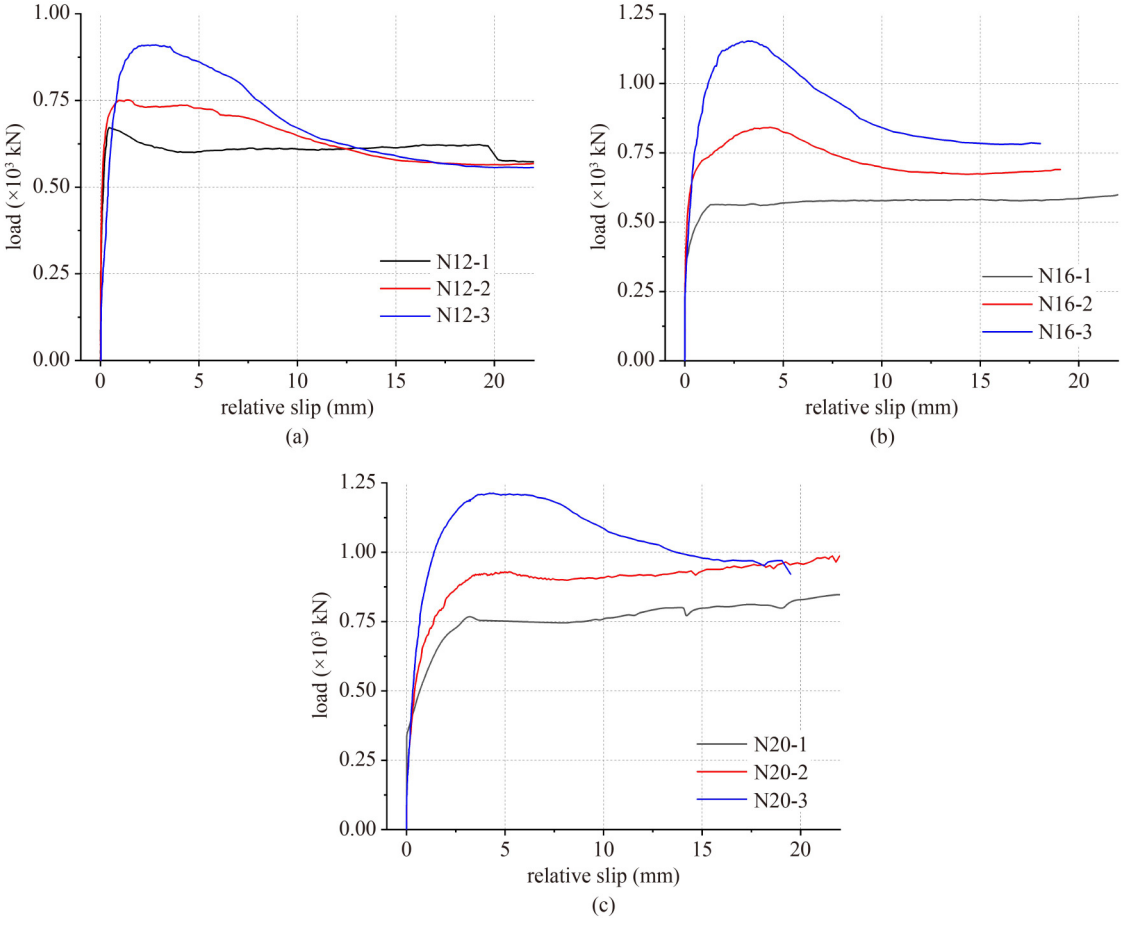

Fig. 4 Load−slip curve: (a) N12; (b) N16; (c) N20.

holes in the perforated steel plates did not change the trend of the load-displacement curve, but affected the deformation that could be tolerated at different stages. The more the diameter of the reinforcement or the number of holes in the perforated steel plate, the more the structure was subjected to loads in the elastic stage. The larger the diameter of the reinforcement, the bigger the relative slip of the structure. Similarly, the more the number of holes, the bigger the relative slip.

3.3 The shear strength

The shear strength of the specimen is shown in Fig. 5. As the number of holes increased, the ultimate load on the specimen increased. The shear strength increased continuously with the increase in the number of holes. Compared to specimen N12-1, the shear strengths of specimens N12-2 and N12-3 increased by 78.45 and 159.78 kN, respectively. In contrast to specimen N16-1, the shear strengths of specimens N16-2 and N16-3 increased by 178.24 and 310.91 kN, respectively. As compared to specimen N20-1, the shear strengths of specimens N20-2 and N20-3 increased by 141.9 and 215.3 kN, respectively. Similarly, as the diameter of the reinforcement in the hole increased, the ultimate load increased.

4 Calculation method

4.1 Traditional bearing capacity calculation model

To determine the factors affecting shear property, previous research references were further investigated. Scholars have investigated the shear bearing capacity mechanism of PRSCs and have proposed empirical equations for shear bearing capacity based on their respective tests. Considering the effects of concrete at the end-bearing zone, transverse reinforcement and concrete in the hole, Eqs. (1) and (2) have been proposed [12]:

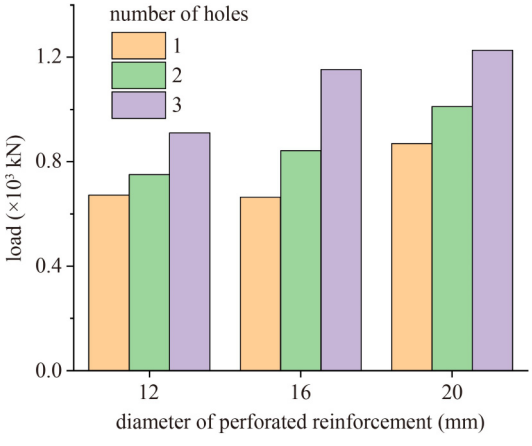

Fig. 5 The ultimate load of the specimens.

$$q_u = 0.59A_{cc}\sqrt{f_c} + 1.233A_{tr}f_y + 2.871nD^2\sqrt{f_c}, \quad (1)$$

$$q_u = 4.5h_{sc}t_{sc}f_c + 0.91A_{tr}f_y + 3.31nD^2\sqrt{f_c}, \quad (2)$$

where q_u is predicted shear strength of PRSC (kN), A_{cc} is concrete shear area (mm^2), A_{tr} is total area of bars (mm^2), f_y is yield stress of the bars (MPa), n is the number of holes, D is the diameter of hole (mm), f_c is the compressive strength of concrete (MPa), h_{sc} is connector height (mm), t_{sc} is connector thickness (mm). Ahn et al. [43] has proposed that the influence of transverse reinforcement on the shear bearing capacity mainly comes from the perforating reinforcement in the hole. Equation (2) was modified and the following formula was proposed by Ahn:

$$q_u = 3.14h_{sc}t_{sc}f_c + 1.21A_{tr,r}f_{y,r} + 2.98nD^2\sqrt{f_c}, \quad (3)$$

where $A_{tr,r}$ is area of bars in holes (mm^2), $f_{y,r}$ is yield stress of bars in holes (MPa). Medberry and Shahrooz [44] believed that the bonding force would also affect the shear capacity of the structure, and proposed the following formula:

$$q_u = 0.747bh\sqrt{f_c} + 0.413b_fL_c + 0.9A_{tr}f_y + 1.66n\pi\left(\frac{D}{2}\right)^2\sqrt{f_c}, \quad (4)$$

where h is slab length in the front of connector (mm), b is concrete slab thickness (mm), b_f is width of the steel section flange (mm), L_c is contact length between the concrete and steel section (mm). Yang and Chen [45] modified the calculation of concrete in holes and took into account the effect of distance between holes on bearing capacity:

$$\begin{cases} P_u = 5.15h_{sc}t_{sc}f_c + 5.41\eta(A_D - A_{tr,r})f_c^{0.57} + 2.24\eta A_{tr,r}f_{y,r}, \\ \eta = \dfrac{nD}{(n-1)e}, \ (n \geqslant 2) \end{cases} \quad (5)$$

where η is the reduction factor, e is the distance between holes. Veríssimo et al. [46] proposed Eq. (6) to calculate the shear strength:

$$q_u = 4.04\frac{h_{sc}}{b}h_{sc}t_{sc}f_c + 2.37nD^2\sqrt{f_c} + 0.16A_{cc}\sqrt{f_c} + 31.85\times10^6\frac{A_{tr}}{A_{cc}}. \quad (6)$$

In summary, the shear bearing capacity of PRSCs is mainly divided into the following parts: compressive bearing capacity of concrete at the end-bearing zone, shear bearing capacity of concrete at the end-bearing zone, shear bearing capacity of concrete in holes, yield strength of transverse reinforcement (including perforating reinforcement in the hole and other transverse reinforcement) and the bonding force between steel plate

and concrete. The number of perforated plates (α_p) also affects the shear strength. According to the above equation, α, f_c, bh, $h_{sc}t_{sc}$, A_{cc}, b_fL_c, n, D, η, α_p, $A_{tr}f_y$ and $A_{tr,r}f_{y,r}$ were selected as the influencing factors of shear capacity in this paper, as shown in Fig. 6.

To verify the reliability of the calculation equation, 107 data were selected according to this paper and previous references [6–12,16,36]. The statistical parameters of the data are shown in Table 2. Where, q_e is the experimental value of shear strength, μ is average value, SD is standard deviation, CV is coefficient of variation. The values of SD and CV are both large, indicating that the data of each influencing parameter is scattered.

The error distribution of each equation is shown in Table 3. The calculation error of the equation is significant. The average error of Eq. (1) is 93%, and only 59% of the calculated results have an error rate less than 100%. The average error of Eqs. (2) and (4) is greater than 50%, and the error of most of the calculated results is greater than 50%. The average errors of Eqs. (3) and (5) plural greater than 30%, and the errors of some calculation results plural more than 50%. In brief, the equations proposed for calculating the shear capacity of PRSC depend on their tests and do not fully consider the effects of various factors. Therefore, it is necessary to find a new calculation method.

4.2 Computational method based on ANN model

The ANN model is a calculation model based on the structure and function of a biological neural network. The ANN model is shown in Fig. 7. Due to the powerful ability of ANN to learn complex relationships when functional relationships are not transparent, using this method in numerical simulation and engineering problem solving has attracted more and more interest. This paper chooses back propagation (BP)-ANN and BP-ANN based on genetic algorithm optimization (GABP-ANN) for calculation. BP-ANN is a multi-layer feedforward network trained by error back propagation.

GA is a parallel stochastic search optimization method proposed based on the simulation of genetic mechanism

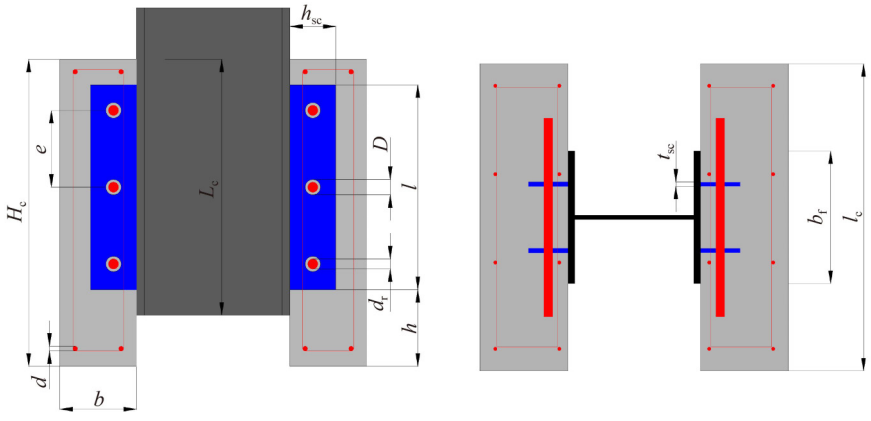

Fig. 6 Parameters of the PRSC.

Table 2 Test data statistics

parameter	max	min	μ	SD	CV
α	1	0	0.8	0.4	0.49
f_c (MPa)	70.3	20.91	40.25	13.34	0.33
bh (mm^2)	80000	15000	37745.84	16508.99	0.44
$h_{sc}t_{sc}$ (mm^2)	4800	774	1868.58	933.54	0.5
b_fL_c (mm^2)	210000	96000	131550.47	26449.42	0.2
n	4	0	2.14	1.21	0.57
D (mm)	90	0	47.76	17.52	0.37
η	1	0.3	0.77	0.21	0.27
α_p	2	1	1.31	0.46	0.35
$A_{tr}f_y$ (N)	1281769.79	0	424540.92	312684.08	0.74
$A_{tr,r}f_{y,r}$ (N)	738902.58	0	104737.55	146890.91	1.4
q_e	2066.7	179.4	589.9	362.22	0.61

Table 3 The absolute error distribution of the equation

absolute error (%)	Eq. (1)	Eq. (2)	Eq. (3)	Eq. (4)	Eq. (5)
0–10	9%	20%	18%	12%	19%
10–20	7%	14%	13%	10%	25%
20–30	13%	9%	13%	9%	15%
30–40	7%	7%	18%	12%	12%
40–50	7%	6%	23%	5%	4%
50–60	1%	7%	12%	5%	5%
60–70	3%	4%	3%	4%	5%
70–80	3%	6%	0%	5%	3%
80–90	3%	6%	0%	4%	5%
90–100	6%	7%	0%	4%	0%
average	93%	55%	35%	59%	31%

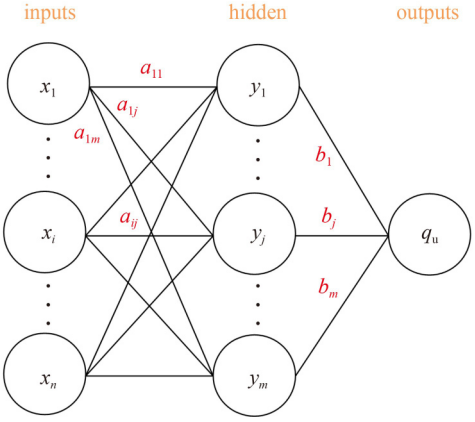

Fig. 7 ANN model.

in nature and biological evolution theory. GABP-ANN consists of three parts: determination of neural network structure, optimization and prediction. The essential idea is that the initial weights and thresholds of the network are represented by individuals, and the prediction errors of the BP-ANN are used to represent the fitness values of the individuals. Finally, the optimal initial weights are found by selection, crossover and variation operations. The purpose of GABP-ANN is to improve the initial weights and thresholds of the network by GA, so that the optimized model can make better predictions.

In order to determine the appropriate neural network model, different models are compared. The specific calculation process is shown in Fig. 8. The computational process mainly includes selection of neural network, selection of input parameters, comparison of neural network models, parameter sensitivity analysis based on the ANN models and selection of final neural network.

When the number of nodes in the input layer and output layer is fixed, choosing the appropriate number of layers and the number of nodes in the hidden layer has a great impact on the performance of the neural network. In order to better compare the hybrid algorithm in this work with the single BP-ANN, a single hidden layer was used for the prediction model of both algorithms. The number of neurons in the hidden layer is determined following a trial-and-error procedure [47], the accuracy of the ANN was tested by comparing the different numbers of neurons in the hidden layer and the best number of neurons with the largest R^2 output was selected for further investigation. Therefore, the optimal number of neurons was different for the different models investigated in this study. The hidden layer neuron transfer function used the S-shaped tangent function "tansig", and the output layer neuron transfer function used the S-shaped logarithmic function "logsig". The model was trained with the function "trainlm". During training, the minimum error of the training target was 1.0×10^{-5}, the maximum number of training steps was 10000, and the learning rate was 0.01. The behavior of a GA was controlled by a set of hyperparameters, such as population size and mutation rate. With a small population size, it is clear that inbreeding will occur, producing pathological genes that prevent the population from evolving to produce the desired population size as expected by the model theorem. If the population size is too large then the results are difficult to converge and wasteful of resources, with reduced robustness. If the mutation probability is too small, the diversity of the population decreases too quickly, leading to rapid loss of effective genes. If the mutation probability is too large, although the diversity of the population can be ensured, the probability of disruption of higher order patterns increases. Similar to the variation probability, when the crossover probability is too large, it tends to destroy the existing favorable pattern, and so increasing the randomness and missing the optimal individuals. Too small crossover probability cannot effectively update the population. If the evolutionary algebra is too small, the algorithm does not converge easily and the population is not yet mature. If the evolutionary algebra is too large, the algorithm is already proficient or the population is too early to converge, and there is no point in continuing the evolution, which will only increase the time expenditure and waste of resources. Based on the above issues, the values of the parameters are shown in Table 4.

The selection process of input parameters is shown in Subsection 4.1. Among them, 90 data are chosen as training data, and 22 data are chosen as test data. The data is divided based on the condition that the training and test datasets have the same statistical distribution, rather than being divided randomly. The data statistics are shown in Table 5.

To judge the effect of each parameter on shear strength, the input parameters are combined according to Eqs. (1)–(5) to establish different ANN models. The input parameters of the BP-0–BP-5 ANN models and GABP-0–GABP-5 ANN models are directly combined

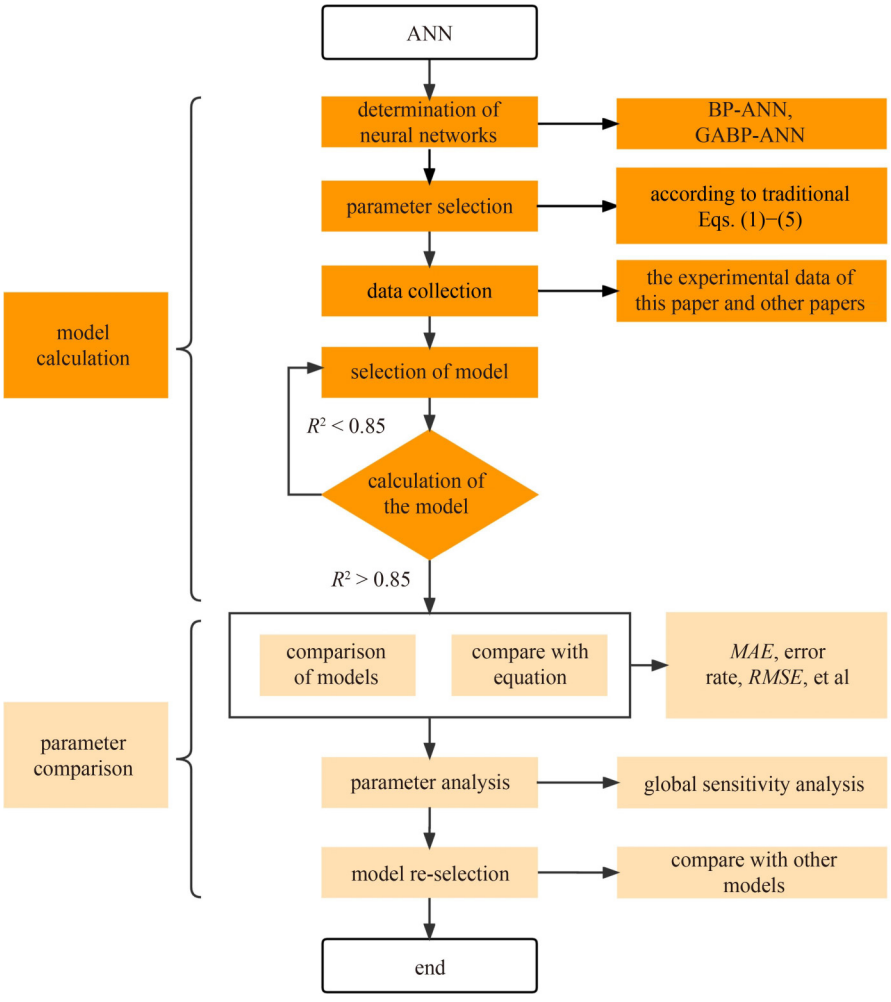

Fig. 8 Calculation process of ANN.

Table 4 Parameters of the GA

population size	crossover probability	mutation probability	evolutionary algebra
50	0.6	0.05	100

from the 11 parameters determined in Subsection 4.1. To decrease the number of input variables, the bearing capacity of PRSC is expressed by combining 11 parameters based on empirical equations. The combined parameters based on the equations are used as input parameters for the BP-6–BP-11 ANN models and GABP-6–GABP-11 ANN models. Input parameters are shown in Table 6.

4.3 Global sensitivity analysis—ANN model

Different input parameters may change the output results of the ANN model, so the degree of influence of the input parameters on the shear strength needs to be quantified. Sensitivity analysis is frequently used to determine the importance of input variables and to describe their effects on the dependent variable. Sensitivity analysis is divided into local sensitivity analysis and GSA. GSA can analyze the effect of multiple variables on the overall results of

Table 5 Test data statistics of training data and testing data

parameter	training data			testing data		
	max	min	μ	max	min	μ
α	1	0	0.8	1	0	0.84
f_c (MPa)	70.3	20.91	35.23	70.3	20.91	44.31
bh (mm^2)	80000	15000	37235	80000	15000	33748
$h_{sc}t_{sc}$ (mm^2)	4800	774	1867	4000	774	1876
$b_l L_c$ (mm^2)	210000	96000	131525	210000	96000	137348
n	4	0	2.15	4	0	2
D(mm)	90	0	47.11	60	0	46.23
η	1	0.44	0.78	1	0.44	0.8
α_p	2	1	1.31	2	1	1.33
$A_{tr}f_y$ (N)	1281769	0	433547	915678	0	426456
$A_{tr,r}f_{y,r}$ (N)	738902	0	103452	376461	0	111245
q_e	2066.7	179.4	593.66	1118.3	179.4	535.56

Table 6 ANN models

model	input parameters
BP-0	$\alpha, f_c, f_c^{0.5}, bh, h_{sc}t_{sc}, b_fL_c, n, D, \eta, \alpha_p, A_{tr}f_y, A_{tr,r}f_{y,r}$
GABP-0	
BP-1	$\alpha, f_c^{0.5}, bh, n, D, \alpha_p, A_{tr}f_y$
GABP-1	
BP-2	$\alpha, f_c, f_c^{0.5}, h_{sc}t_{sc}, n, D, \alpha_p, A_{tr}f_y$
GABP-2	
BP-3	$\alpha, f_c, f_c^{0.5}, h_{sc}t_{sc}, n, D, \alpha_p, A_{tr,r}f_{y,r}$
GABP-3	
BP-4	$\alpha, f_c^{0.5}, bh, b_fL_c, n, D, \alpha_p, A_{tr}f_y,$
GABP-4	
BP-5	$\alpha, f_c, f_c^{0.57}, h_{sc}t_{sc}, n, D, \eta, \alpha_p, A_{tr,r}f_{y,r}, A_{tr,r}$
BP-6	$\alpha bh f_c^{0.5}, b_fL_c, \alpha h_{sc}t_{sc}f_c, nD^2f_c^{0.5}, A_{tr}f_y, A_{tr,r}f_{y,r}, \alpha_p$
GABP-6	
BP-7	$\alpha bh f_c^{0.5}, nD^2f_c^{0.5}, A_{tr}f_y, \alpha_p$
GABP-7	
BP-8	$\alpha h_{sc}t_{sc}f_c, nD^2f_c^{0.5}, A_{tr}f_y, \alpha_p$
GABP-8	
BP-9	$\alpha h_{sc}t_{sc}f_c, nD^2f_c^{0.5}, A_{tr,r}f_{y,r}, \alpha_p$
GABP-9	
BP-10	$\alpha bh f_c^{0.5}, b_fL_c, A_tf_y, nD^2f_c^{0.5}, \alpha_p$
GABP-10	
BP-11	$\alpha h_{sc}t_{sc}f_c, \eta(0.785nD^2 - A_{tr,r})f_c^{0.57}, \eta A_{tr,r}f_{y,r}, \alpha_p$

the model, and determine the effect of each variables and the influence of their interaction on the result.

This paper uses Sobol's method, a variance-based sensitivity analysis method. Sobol's method can be used for non-linear, non-monotonic mathematical models with reliable results. The method is able to determine significant variables and assess the degree of their influence on the corresponding results. A critical characteristic of this method is the randomized treatment of the input variables. The core idea is based on the decomposition of variance, decomposing the function model into individual parameters and combinations between parameters, and performing sensitivity analysis of parameters by calculating the output variance of individual input parameters or a set of input parameters.

Assume that the model is $Y = f(x)$, $x = [x_1, x_2, \ldots, x_k]$. x is a data set established based on Latin hypercube sampling and a neural network model, the upper and lower limits of each parameter are determined according to Table 5. $f(x)$ is as follows:

$$f(x) = f_0 + \sum_{i=1}^{k} f_i(x_i) + \sum_{1<i<j\leqslant k} f_{i,j}(x_i, x_j) + \cdots + f_{1,2,\ldots,k}(x_1, x_2, \ldots, x_k), \tag{7}$$

where $\sum_{i=1}^{k} f_i(x_i)$ is the sum of the main effect functions, and $\sum_{1<i<j\leqslant k} f_{i,j}(x_i, x_j) + \cdots + f_{1,2,\cdots,k}(x_1, x_2, \ldots, x_k)$ is the sum of all interactions. If the above equation holds, the following characteristics must be satisfied:

$$\int_0^1 f_{i_1,i_2,\cdots,i_n}(x_{i1}, \ldots, x_{in})\,\mathrm{d}x_{ij} = 0,\ 1 \leqslant j \leqslant n. \tag{8}$$

The Sobol decomposition term in Eq. (7) can be obtained:

$$f_0 = \int_0^1 f(x)\mathrm{d}x, \tag{9}$$

$$f_i(x_i) = \int_0^1 \cdots \int_0^1 f(x)\mathrm{d}x_{-i} - f_0, \tag{10}$$

$$f_{ij}(x_i, x_j) = \int_0^1 \cdots \int_0^1 f(x)\mathrm{d}x_{-(i,j)} - f_0 - f_i(x_i) - f_j(x_j), \tag{11}$$

where $f(x_i)$ represents the marginal effect, $\int_0^1 \cdots \int_0^1 f(x)\mathrm{d}x_{-i}$ is integrating with respect to all variables, except x_i. The total variance (V) is calculated as follows:

$$V = Var[f(x)] = \int_0^1 f^2(x)\mathrm{d}x - f_0^2 = E[f^2(x)] - E[h(x)]^2, \tag{12}$$

where $E[\cdot]$ is expected value, $Var[\cdot]$ is variance. The partial ($V_{i_1,\ldots,i_s}$) and total variances can be calculated as follows:

$$V_{i_1,\ldots,i_s} = \int_0^1 \cdots \int_0^1 h^2_{i_1,\ldots,i_n}(x_{i_1}, \ldots, x_{i_s})\,\mathrm{d}x_{i_1} \cdots \mathrm{d}x_{i_n}, 1 \leqslant i_s \leqslant k, \tag{13}$$

$$V = \sum_{i=1}^{n} V_i + \sum_{1\leqslant i<j\leqslant n} V_{ij} + \cdots + V_{1,2,\ldots,n}. \tag{14}$$

The Sobol indices including first-order (S_i) and total-order (S_{Ti}) is done with the following equations:

$$S_i = \frac{V_{i_1,\ldots,i_s}}{V} = \frac{Var(f(x)) - E_x[Var_{x_{\sim i}}(f(x) \mid x_i)]}{Var(f(x))}, \tag{15}$$

$$S_{Ti} = 1 - \frac{V_{\sim i}}{V} = \frac{Var_{x_{\sim j}}[E_{x_i}(f(x) \mid x_{\sim i})]}{Var(f(x))}, \tag{16}$$

where $V_{\sim i}$ is the variance of all input parameters except ith, $x_{\sim i}$ is all but the ith input factor. S_i is the main effect. S_{Ti} is all contributions of the input variable to the output variance. GSA methods provide valuable insights, but their application needs large amounts of data. To solve the problem of insufficient data, a large amount of

reliable data is generated by neural networks. Instead of functional equations, ANN models are used to generate the required independent variables.

5 Analysis of prediction results

5.1 Prediction results based on ANN model

The network performance for the training and testing datasets of the neural network is shown in Fig. 9. The training error drops sharply in the early iterations and then stabilizes. Training can continue with negligible improvement. After the error in the test set is reduced, training is allowed to proceed for another 10 iterations, in order to prevent overfitting. The connection weights were chosen to be at the lowest mean squared error of the test set.

The ANN model prediction results of the testing data (for which each model was reinitialized 50 times) are shown in Tables 7 and 8. *MAE* is Mean Absolute Error, it represents the mean of the absolute error between the predicted value and the observed value. *RMSE* is Root Mean Square Error, the larger the error, the greater the value. The absolute error values of all models do not exceed 100 kN, the average absolute error rate does not exceed 20%, the maximum absolute error rate does not exceed 65%, and the R^2 is not less than 0.9, which verifies the accuracy of the prediction results of the neural network model. Forming multiple influences on new variables based on empirical equations reduces the number of input variables but does not significantly change the prediction results of the neural network. The prediction results of models BP-0, BP-6, GABP-0 and GABP-6 outperformed the other models, indicating that the influencing parameters identified in this paper have some effect on the shear strength. Comparing the BP and GABP models of 1, 4, 7 and 10, it can be seen that $b_f L_c$ can affect the prediction results, but the effect is small. Comparing 2, 3, 8 and 9 of the BP and GABP models, it can be seen that $A_{tr} f_y$ and $A_{tr,r} f_{y,r}$ have a relatively large effect on the prediction results. The accuracy of the

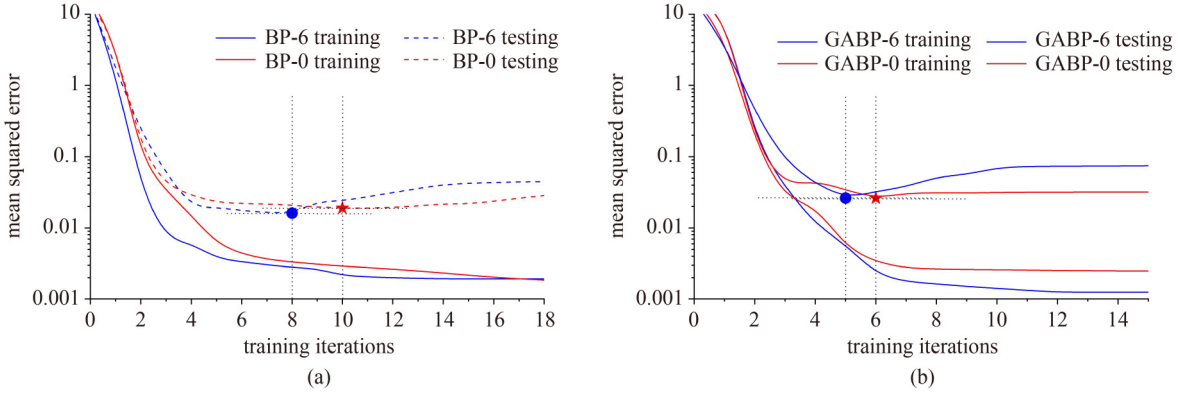

Fig. 9 Comparative convergence analyses of mean squared error in the training and testing datasets: (a) BP model; (b) GABP model.

Table 7 Predicted results of BP model

model	*MAE* (kN)	absolute error rate (%)				*RMSE*	R^2
		average	max	min	*SD*		
BP-0	46.37	12.31	43.39	0.84	10.53	57.71	0.95
BP-1	55.96	12.06	24.65	1.17	6.35	76.17	0.93
BP-2	61.50	14.27	54.11	0.95	12.87	71.97	0.94
BP-3	64.69	11.08	27.13	1.22	8.82	89.25	0.94
BP-4	92.94	19.90	47.45	2.60	13.57	104.64	0.93
BP-5	73.18	17.06	36.95	1.15	15.43	88.20	0.93
BP-6	44.04	9.30	18.19	1.05	4.65	47.52	0.95
BP-7	71.00	16.43	61.55	1.69	15.01	88.13	0.91
BP-8	68.84	16.01	48.18	1.27	12.63	82.90	0.93
BP-9	94.99	17.60	49.88	1.55	12.43	112.22	0.9
BP-10	84.35	16.52	45.63	0.36	13.24	95.38	0.9
BP-11	81.65	15.35	50.35	0.68	15.53	114.34	0.91

GABP model is higher than that of the BP model for the same input variables.

To obtain the best results, 10-fold cross-validation was applied to all models, as shown in Figs. 10 and 11. The average absolute error rate and *RMSE* of the prediction results obtained by the GABP model is always smaller

Table 8 Predicted results of GABP model

model	*MAE* (kN)	absolute error rate (%)				*RMSE*	R^2
		average	max	min	*SD*		
GABP-0	45.22	9.59	31.55	1.42	9.06	60.21	0.95
GABP-1	51.72	11.19	45.78	0.69	12.60	72.63	0.93
GABP-2	53.00	9.73	38.23	0.96	8.10	66.62	0.95
GABP-3	51.27	10.98	26.54	0.54	8.73	66.03	0.96
GABP-4	58.92	13.35	43.54	1.03	11.04	77.94	0.93
GABP-5	47.16	11.68	37.38	0.53	18.53	62.59	0.95
GABP-6	35.97	6.94	14.75	1.09	3.42	40.04	0.98
GABP-7	61.37	13.49	47.80	1.07	13.81	76.50	0.92
GABP-8	56.35	10.15	26.48	1.95	7.70	74.74	0.94
GABP-9	50.11	12.39	24.89	0.76	5.98	57.16	0.93
GABP-10	57.11	13.73	44.29	0.46	9.71	79.96	0.93
GABP-11	75.48	13.17	43.19	0.72	10.23	99.99	0.92

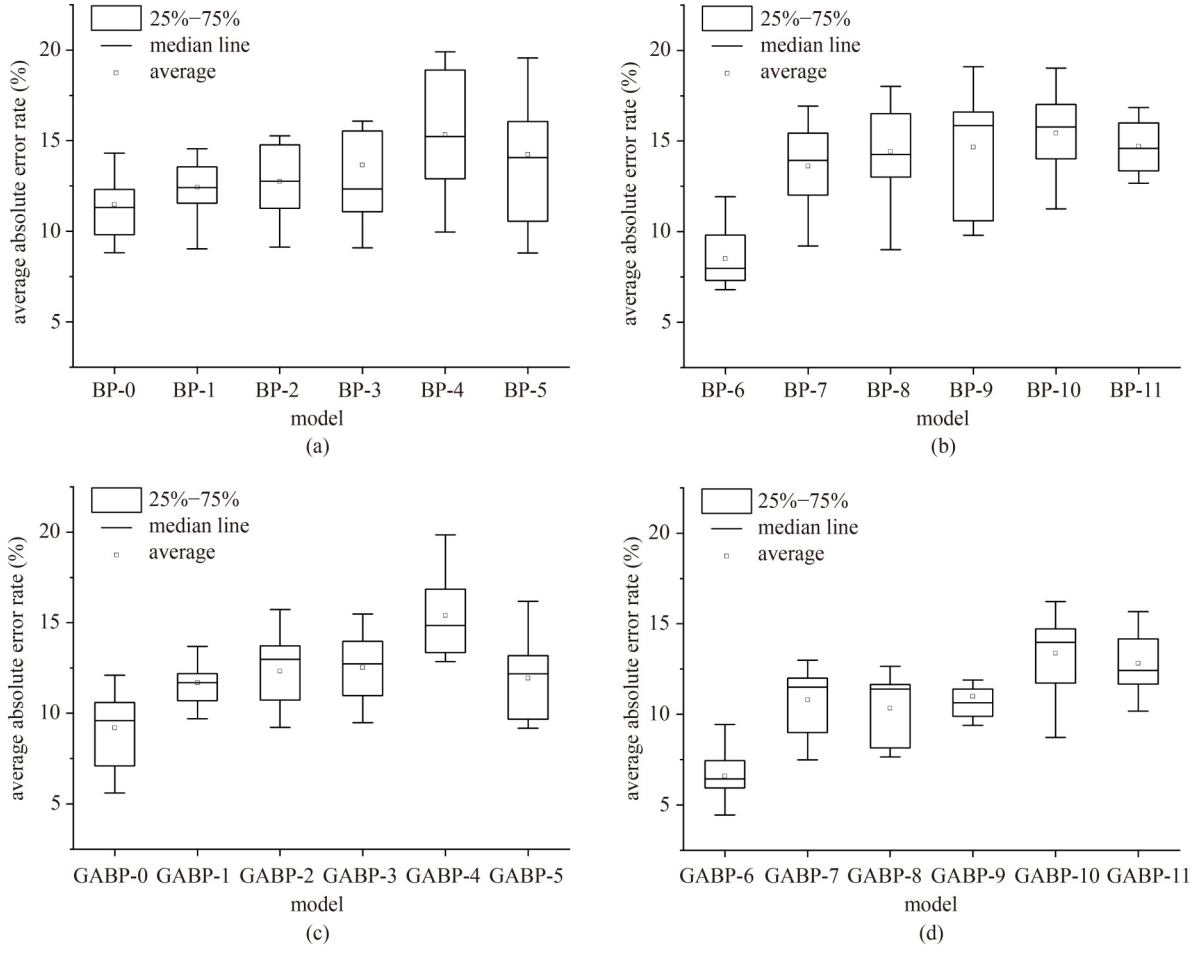

Fig. 10 Average absolute error rate of 10-fold cross-validation: (a) BP-0–BP-5 ANN models; (b) BP-6–BP-11 ANN models; (c) GABP-0–GABP-5 ANN models; (d) GABP-6–GABP-11 ANN models.

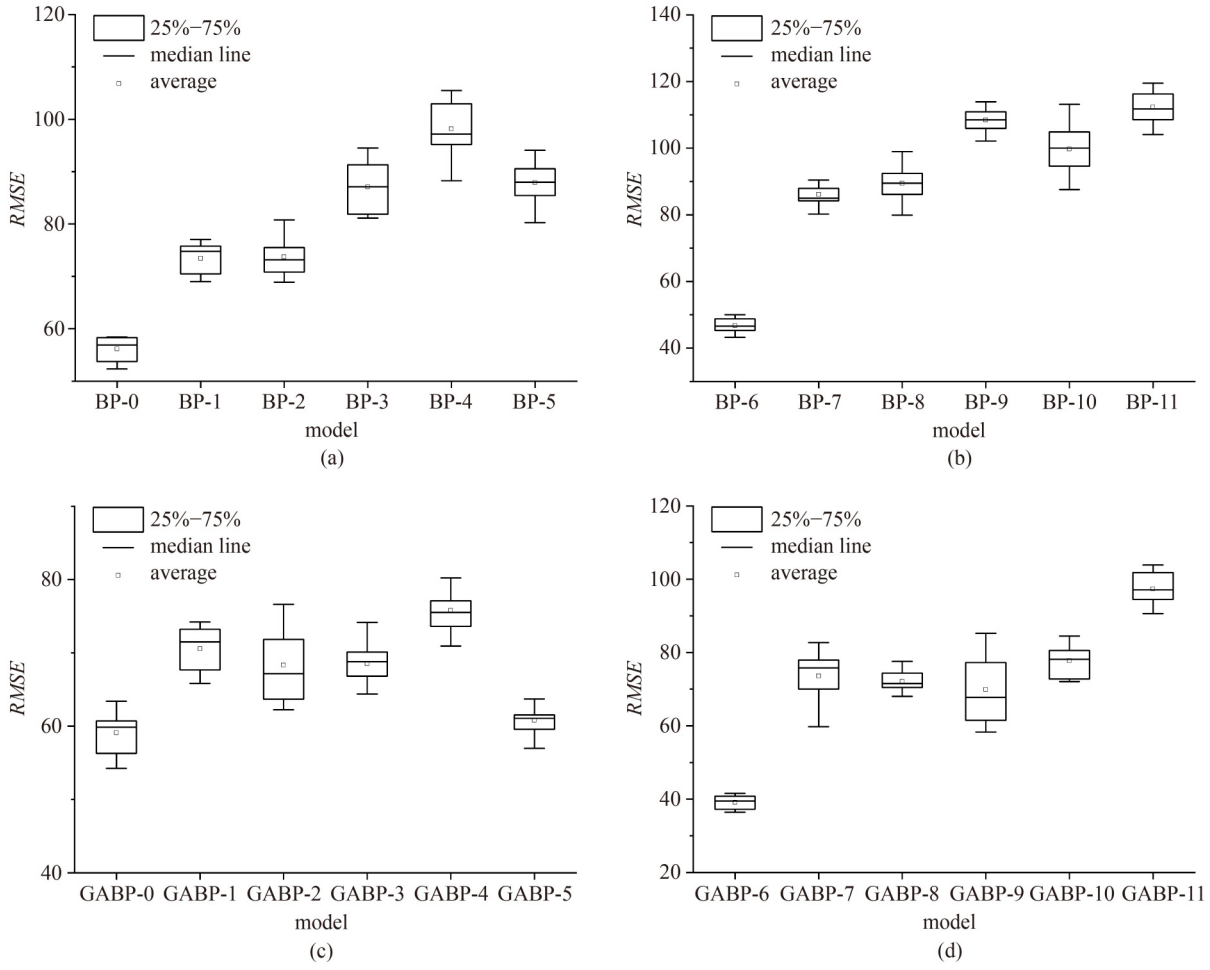

Fig. 11 *RMSE* of 10-fold cross-validation: (a) BP-0–BP-5 ANN models; (b) BP-6–BP-11 ANN models; (c) GABP-0–GABP-5 ANN models; (d) GABP-6–GABP-11 ANN models.

than that obtained by the BP model, which indicates that the prediction accuracy of the BP model can be improved by GA optimization. The average absolute error rate in the test set of the GABP-6 model ranged from 4.4% to 9.4%, which is much lower than the other models. The average absolute error rate of the BP-6 model ranged from 6.8% to 11.9%. In conclusion, the prediction result of ANN model GABP-6 is better than that of other models, so this model is preliminarily selected as the optimal ANN calculation model.

The calculated results from the model and equation are compared, as shown in Fig. 12. The prediction results of ANN model GABP-6 were significantly better than those of the empirical equations. The predicted values of the model GABP-6 were fluctuated up and down around the experimental values, and the absolute error rate of all the prediction results is less than 20%. Equation (2)'s calculated value is mostly higher than the experimental value, while Eq. (3)'s calculated value is mostly lower than the experimental value.

The effect of the parameters on the computational results of the empirical equation and the ANN model is

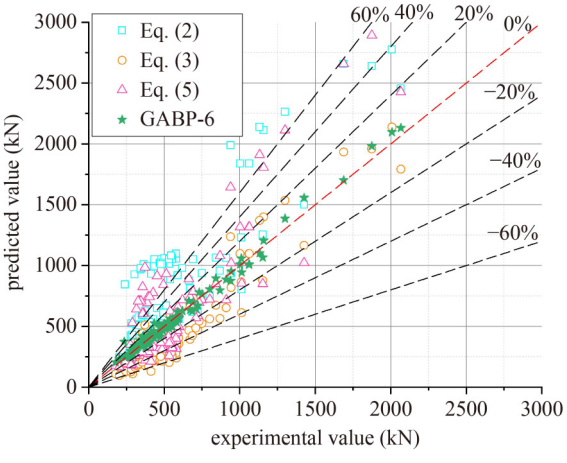

Fig. 12 Prediction results of GABP-6 model and equations.

shown in Fig. 13. The q_e/q_u of the GABP-6 is close to 1 and does not change significantly with the change of parameters. The q_e/q_u calculated by Eq. (2) is less than 1 and does not change significantly with the change of parameters. With the increase of the parameters, the trend

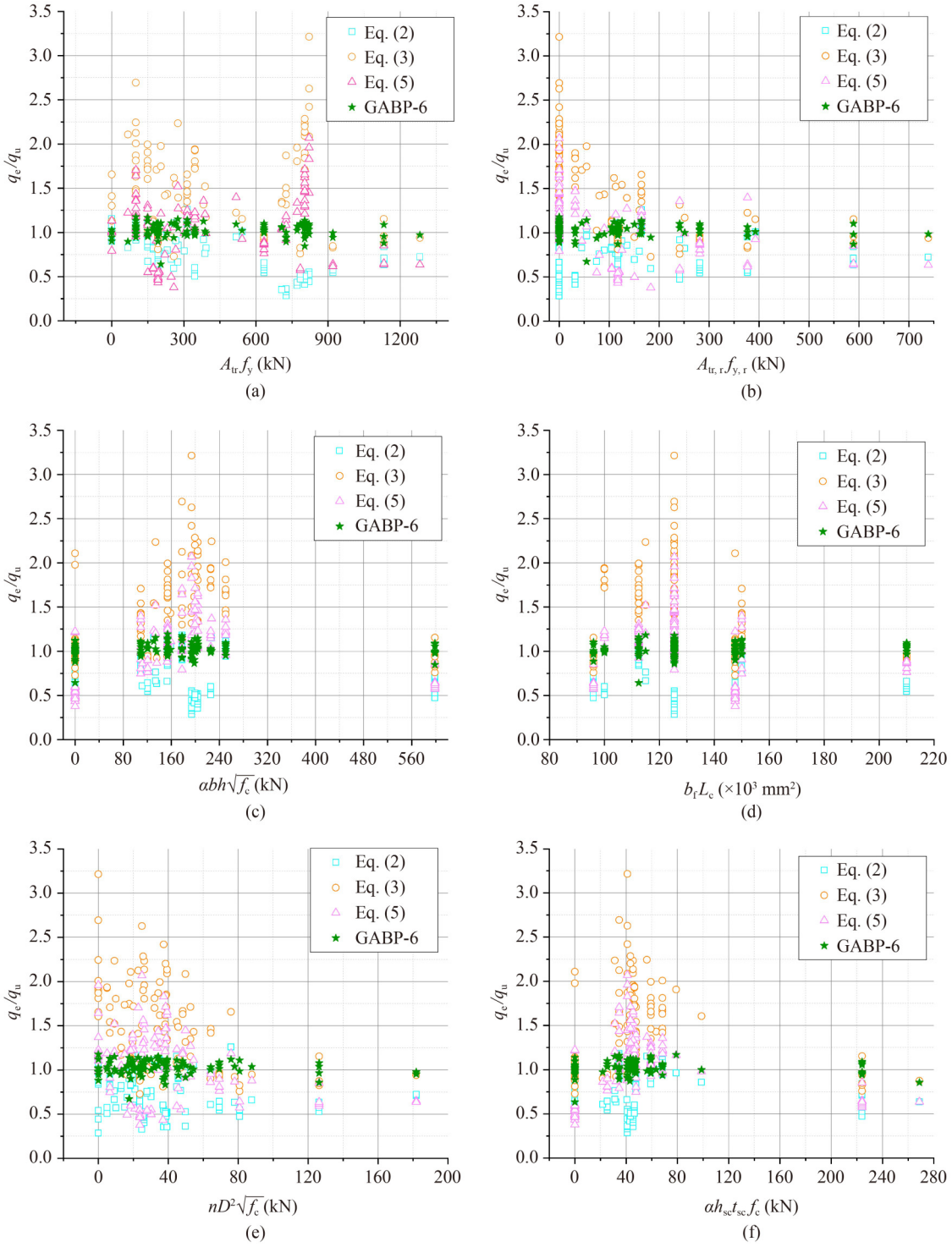

Fig. 13 Prediction results with different input parameters: (a) $A_{tr}f_y$; (b) $A_{tr,r}f_{y,r}$; (c) $\alpha bh\ f_c^{0.5}$; (d) b_fL_c; (e) $nD^2\ f_c^{0.5}$; (f) $\alpha h_{sc}t_{sc}f_c$.

of q_e/q_u calculated by Eq. (3) is changed significantly. With the increase of $A_{tr}f_y$, the q_e/q_u of Eq. (3) changes in a wave shape. With the increase of $A_{tr,r}f_{y,r}$ and $nD^2\ f_c^{0.5}$, the q_e/q_u of Eq. (3) tends to decrease and the prediction results become more and more accurate. As $\alpha bh\ f_c^{0.5}$, b_fL_c and $\alpha h_{sc}t_{sc}\ f_c$ increase, the q_e/q_u of Eq. (3) tends to first increase and then decrease. With the change of parameters, the distribution of q_e/q_u calculated by Eq. (5) did not show a clear rule.

5.2 Analysis results of GSA method—ANN model

Based on the GABP-6 model, 4000 data were generated for the GSA method. To directly analyze the sensitivity of

each factor to shear strength, S_i and S_{Ti} of each factor were normalized. The sensitivity analysis results are shown in Fig. 14. The effect of the penetration reinforcement in the hole having the most significant effect on the shear strength. Concrete also affects the shear performance of PRSCs, where the Sobol index of compressive bearing capacity of concrete in the end bearing area is larger than the shear bearing capacity of concrete in the hole. The shear bearing capacity of concrete at the end-bearing zone and the bonding force have little effect on the shear strength. Hence, to optimize the ANN model, $\alpha h_{sc} t_{sc} f_c$, $nD^2 f_c^{0.5}$, $A_{tr} f_y$, $A_{tr,r} f_{y,r}$ and α_p with larger Sobol indices are selected as input parameters to build new ANN models (BP-12 ANN model and GABP-12 ANN model).

The prediction results of the GABP-12 ANN model and BP-12 ANN model are shown in Fig. 15. Although the input parameters are reduced, the prediction results do not change significantly, and the value of R^2 did not change compared to the model GABP-6. The distribution of prediction results of model GABP-12 is better than BP-12, so GABP-12 is chosen as the final ANN calculation model. Compared with other ANN models, model GABP-12 has fewer input parameters and higher calculation accuracy and can be used to calculate the shear bearing capacity of PRSCs. The two eliminated variables have less influence on the prediction results of the neural network, which verifies the reliability of the GSA method. When all important parameters are used as input variables, the ANN model predicts better results after optimization by the GA method.

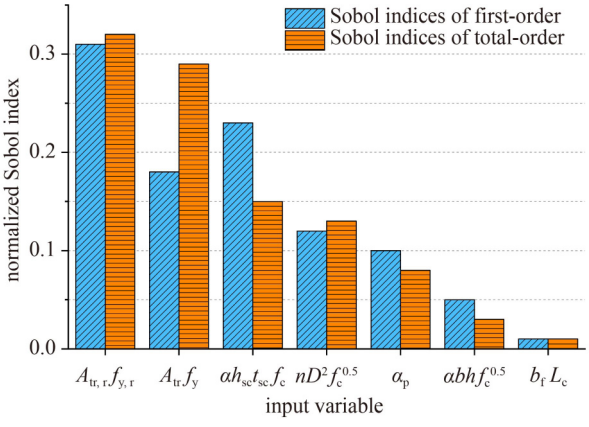

Fig. 14 Analysis results of GSA method.

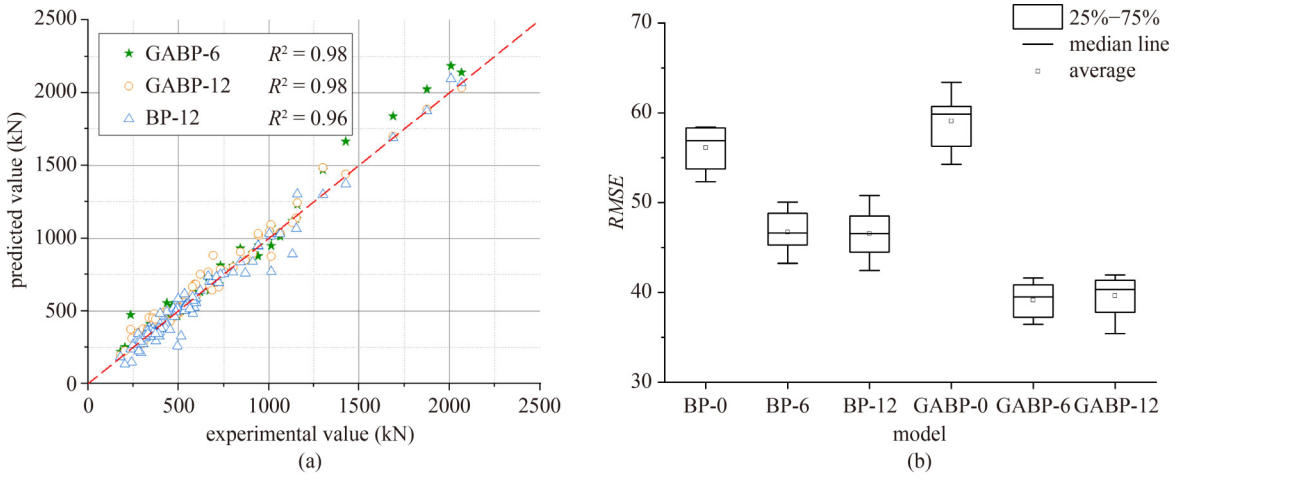

Fig. 15 The predicted results of the modified ANN model: (a) distribution of predicted values; (b) *RMSE* of 10-fold cross-validation.

6 Conclusions

In this paper, the influence of the number of holes in the steel plate and the diameter of the penetrating reinforcement in the holes on PRSC was analyzed, based on push-out test. BP ANN model and GABP ANN model for predicting shear strength were developed, and the shear strength of this experiment was included as part of the test set. The effects of all factors on the shear strength of PRSC were analyzed by the GSA methods based on the ANN model. The major conclusions are as follows.

1) In all tested specimens, the damage modes mainly include concrete slab cracking damage, and yielding damage of reinforcement. When the concrete strength intensity is fixed, the number of holes and the penetrating reinforcement change the damage mode of the specimen.

2) At the peak of the load, the slip of the specimen with more holes is greater than the slip of the specimen with fewer holes. Also, he larger the diameter of the penetration reinforcement, the larger the slip of the specimens. This indicates that the number of holes and the diameter of penetration reinforcement change the performance and ductility of PRSCs.

3) Different input variables affect the prediction results of the ANN model. Forming multiple influences into new variables based on empirical equations reduces the number of input variables but does not significantly change the prediction results of the neural network.

4) The ANN model has a higher computational accuracy than that of the empirical equation, and the ANN model can be used for shear strength prediction of PRSCs, thus reducing the need to conduct expensive experiments. When all important parameters are selected as input variables, the ANN model prediction is improved after optimization by the GA method.

5) A parameter analysis method based on the ANN model and the GSA method is proposed, which can examine the importance of parameters. The results indicate that the sensitivity of the penetrating reinforcement in the hole to the shear strength is the most significant, and the bonding force between steel plate and concrete is the least. The prediction accuracy of the ANN model does not change obviously after removing the variables that have little influence.

References

1. Vigneri V, Odenbreit C, Romero A. Numerical study on design rules for minimum degree of shear connection in propped steel-concrete composite beams. Engineering Structures, 2021, 241(4): 112466
2. Wu F, Liu S, Xue C, Yang K, Feng Y, Zhang H. Experimental study on the mechanical properties of perfobond rib shear connectors with steel fiber high strength concrete. Materials (Basel), 2021, 14(12): 3345
3. Li Z, Zhao C, Deng K, Wang W. Load sharing and slip distribution in multiple holes of a perfobond rib shear connector. Journal of Structural Engineering, 2018, 144(9): 264−276
4. Kim K, Han O, Heo W, Kim S. Behavior of Y-type perfobond rib shear connection under different cyclic loading conditions. Structures, 2020, 26: 562−571
5. Gu J, Liu D, Deng W, Zhang J. Experimental study on the shear resistance of a comb-type perfobond rib shear connector. Journal of Constructional Steel Research, 2019, 158: 279−289
6. Ahn J, Lee C, Won J, Kim S. Shear resistance of the perfobond-rib shear connector depending on concrete strength and rib arrangement. Journal of Constructional Steel Research, 2010, 66(10): 1295−1307
7. Wang X, Zhu B, Cui S, Lui E. Experimental research on PBL connectors considering the effects of concrete stress state and other connection parameters. Journal of Bridge Engineering, 2018, 23(1): 04017125
8. Costa-Neves L, Figueiredo J, Vellasco P, Vianna J. Perforated shear connectors on composite girders under monotonic loading: An experimental approach. Engineering Structures, 2013, 56: 721−737
9. Cândido-Martins J, Costa-Neves L, Vellasco P. Experimental evaluation of the structural response of Perfobond shear connectors. Engineering Structures, 2010, 32(8): 1976−1985
10. Zheng S, Zhao C, Liu Y. Analytical model for load-slip relationship of perfobond shear connector based on push-out test. Materials (Basel), 2018, 12(1): 1−19
11. Leonhardt F, Andrae W, Andrae H, Harre W. New, improved bonding means for composite load bearing structures with high fatigue strength. Beton, 1987, 82(12): 325−331
12. Oguejiofor E, Hosain M. A parametric study of perfobond rib shear connectors. Canadian Journal of Civil Engineering, 1994, 21(4): 614−625
13. Kim S, Kim K, Han O, Park J. Influence of transverse rebar on shear behavior of Y-type perfobond rib shear connection. Construction & Building Materials, 2018, 180: 254−264
14. Manabe Y, Fujiyama C, Kisaku T, Shionaga R. Influence of coarse aggregates on the shear resistance of perfobond rib shear connector. Procedia Engineering, 2014, 95(95): 454−464
15. Su Q, Yang G, Bradford M. Bearing capacity of perfobond rib shear connectors in composite girder bridges. Journal of Bridge Engineering, 2016, 21(4): 06015009
16. Zheng S, Liu Y Q, Yoda T, Lin W. Parametric study on shear capacity of circular-hole and long-hole perfobond shear connector. Journal of Constructional Steel Research, 2016, 117: 64−80
17. Zheng S, Zhao C, Liu Y. Experimental shear strength evaluation of perfobond shear connector with various hole shapes. Structural Engineering and Mechanics, 2018, 67(2): 131−142
18. Garzón-Roca J, Marco C, Adam J. Compressive strength of masonry made of clay bricks and cement mortar: Estimation based on Neural Networks and Fuzzy Logic. Engineering Structures, 2013, 48: 21−27
19. Tzuc O, Gamboa O, Rosel R, Poot M, Edelman H, Torres M J, Bassam A. Modeling of hygrothermal behavior for green facade's concrete wall exposed to nordic climate using artificial intelligence and global sensitivity analysis. Journal of Building Engineering, 2021, 33: 101625
20. Sadrossadat S, Cao Y, Zhang Q. Parametric modeling of microwave passive components using sensitivity-analysis-based adjoint neural-network technique. IEEE Transactions on Microwave Theory and Techniques, 2013, 61(5): 1733−1747
21. Bernus A, Ottlé C, Raoult N. Variance based sensitivity analysis of FLake lake model for global land surface modeling. Journal of Geophysical Research. Atmospheres, 2021, 126(8): 1−19
22. Zamanian S, Terranova B, Shafieezadeh A. Significant variables affecting the performance of concrete panels impacted by wind-borne projectiles: A global sensitivity analysis. International Journal of Impact Engineering, 2020, 144: 103650
23. Guo H, Zhuang X, Rabczuk T. A deep collocation method for the bending analysis of Kirchhoff plate. Computers, Materials & Continua, 2019, 59(2): 433−456
24. Anitescu C, Atroshchenko E, Alajlan N, Rabczuk T. Artificial neural network methods for the solution of second order boundary value problems. Computers, Materials & Continua, 2019, 59(1): 345−359
25. Samaniego E, Anitescu C, Goswami S, Nguyen-Thanh V M, Guo H, Hamdia K, Zhuang X, Rabczuk T. An energy approach to the solution of partial differential equations in computational mechanics via machine learning: Concepts, implementation and applications. Computer Methods in Applied Mechanics and Engineering, 2020, 362: 112790
26. Zhuang X, Guo H, Alajlan N, Zhu H, Rabczuk T. Deep autoencoder based energy method for the bending, vibration, and

buckling analysis of Kirchhoff plates with transfer learning. European Journal of Mechanics. A, Solids, 2021, 87: 104225
27. Guo H, Zhuang X, Chen P, Alajlan N, Rabczuk T. Stochastic deep collocation method based on neural architecture search and transfer learning for heterogeneous porous media. Engineering with Computers, 2022, 1−26
28. Guo H, Zhuang X, Chen P, Alajlan N, Rabczuk T. Analysis of three-dimensional potential problems in non-homogeneous media with physics-informed deep collocation method using material transfer learning and sensitivity analysis. Engineering with Computers, 2022, 1−22
29. Safa M, Shariati M, Ibrahim Z, Toghroli A, Nor N M, Petkovic D. Potential of adaptive neuro fuzzy inference system for evaluating the factors affecting steel-concrete composite beam's shear strength. Steel and Composite Structures, 2016, 21(3): 679−688
30. Chahnasir E S, Zandi Y, Shariati M, Dehghani E, Toghroli A, Mohamed E T, Shariati A, Safa M, Wakil K, Khorami M. Application of support vector machine with firefly algorithm for investigation of the factors affecting the shear strength of angle shear connectors. Smart Structures and Systems, 2018, 22(4): 413−424
31. Hamdia K M, Zhuang X, Rabczuk T. An efficient optimization approach for designing machine learning models based on genetic algorithm. Neural Computing & Applications, 2021, 33(6): 1923−1933
32. Sedghi Y, Zandi Y, Shariati M, Ahmadi E, Azar V M, Toghroli A, Safa M, Mohamad E T, Khorami M, Wakil K. Application of ANFIS technique on performance of C and L shaped angle shear connectors. Smart Structures and Systems, 2018, 22(3): 335−340
33. Toghroli A, Mohammadhassani M, Suhatril M, Shariati M, Ibrahim Z. Prediction of shear capacity of channel shear connectors using the ANFIS model. Steel and Composite Structures, 2014, 17(5): 623−639
34. Shariati M, Mafipour M, Mehrabi P, Bahadori A, Zandi Y, Salih M N A, Nguyen H, Dou J, Song X, Poi-Ngian S. Application of a hybrid artificial neural network-particle swarm optimization (ANN-PSO) model in behavior prediction of channel shear connectors embedded in normal and high-strength concrete. Applied Sciences (Basel, Switzerland), 2019, 9(24): 5534
35. Allahyari H, Nikbin I, Rahimi S, Heidarpour A. A new approach to determine strength of Perfobond rib shear connector in steel-concrete composite structures by employing neural network. Engineering Structures, 2018, 157: 235−249
36. Khalaf J A, Majeed A A, Aldlemy M S, Ali Z H, Al Zand A W, Adarsh S, Bouaissi A, Hameed M M, Yaseen Z M. Hybridized deep learning model for perfobond rib shear strength connector prediction. Complexity, 2021, 2021(8): 1−21
37. Pianosi F, Beven K, Freer J, Hall J W, Rougier J, Stephenson D B, Wagener T. Sensitivity analysis of environmental models: A systematic review with practical workflow. Environmental Modelling & Software, 2016, 79: 214−232
38. Sobol I. Sensitivity estimates for nonlinear mathematical models. Mathematical Modeling & Computational Experiment, 1993, 1(4): 407−414
39. Homma T, Saltelli A. Importance measures in global sensitivity analysis of nonlinear models. Reliability Engineering & System Safety, 1996, 52(1): 1−17
40. Zamanian S, Terranova B, Shafieezadeh A. Significant variables affecting the performance of concrete panels impacted by wind-borne projectiles: A global sensitivity analysis. International Journal of Impact Engineering, 2020, 144: 103650
41. EN1994-1-1. Eurocode4: Design of Composite Steel and Concrete Structures. Brussels: European Committee for Standardization, 2004
42. DB 41/T 696-2011. Technical Standard for Construction of Highway Waveform Steel Web Prestressed Concrete Box Girder Bridge Bracing Method. Henan: Henan Provincial Bureau of Quality and Technical Supervision, 2011
43. Ahn J, Kim S, Jeong Y. Shear behaviour of perfobond rib shear connector under static and cyclic loadings. Magazine of Concrete Research, 2008, 60(5): 347−357
44. Medberry S, Shahrooz B. Perfobond shear connector for composite construction. Engineering Journal (New York), 2002, 39: 2−12
45. Yang Y, Chen Y. Experimental study on mechanical behavior of PBL shear connectors. Journal of Bridge Engineering, 2018, 23(9): 04018062
46. Veríssimo G, Paes J, Valente I, Cruz P, Fakury R. Design and experimental analysis of a new shear connector for steel and concrete composite structures. In: 3rd International Conference on Bridge Maintenance, Safety and Management. Porto: IABMAS, 2006
47. Guan C, Duan Y, Zhai J, Han D. Hydraulic dynamics in split fuel injection on a common rail system and their artificial neural network prediction. Fuel, 2019, 255: 115792